ICA 2019 AACHEN

PROCEEDINGS of the
23rd International Congress on Acoustics

9 to 13 September 2019 in Aachen, Germany

Experiments on self-excited thermoacoustic oscillations in an air-filled closed tube

Nobumasa SUGIMOTO[1]; Keisuke MINAMIGAWA

Department of Pure and Applied Physics, Kansai University, Japan

ABSTRACT

Experiments are performed to demonstrate experimentally emergence of self-excited thermoacoustic oscillations of an air column in a closed, straight tube. Installing therein a stack subjected to a temperature gradient, onset of instability and ensuing self-excited oscillations are investigated. Effects of a pore radius in the stack are examined by using four stacks of 50, 100, 200 and 300 cells per square inches. The onset of instability is discussed in light of the marginal condition derived based on Rott equation. It is found that the temperature ratios at hot-to-cold ends of the stack are higher in all cases than the ones predicted by the marginal conditions. The pressure profiles in the steady-state oscillations exhibit typical characteristics of nonlinear oscillations, i.e. sharp and narrow crests and flat and wide troughs due to many higher harmonics in oscillations, but no shocks appear. A mean pressure is higher near the closed ends. Among the four stacks, it is observed that the peak-to-peak pressure at the closed end takes the maximum 10% relative to the atmospheric pressure in the case of the stack of 100 cells.

Keywords: Thermoacoustics, Self-excited oscillations, Stack, Standing wave

1. INTRODUCTION

Thermoacoustics has attracted continual attention since 19th century but in a relatively special area in acoustics. This may be seen in that few textbooks and monographs in acoustics deal with this subject. However it appears to be gaining status recently as one area in physical acoustics. Thermoacoustic phenomena may be classified into two categories. One is the phenomena due to instability by unsteady heat release like in combustion, while the other is those due to instability of steady heat flow. Of course, it is noted that thermoacoustic phenomena occurring in reality may involve both aspects in the two categories. Nevertheless, unfortunately, researches and communications are closed within each category and have been done independently so far. Recently, however, a new trend toward fusion appears to be born (1).

This paper concerns with the phenomena in the latter experimentally in the simplest situation. Spontaneous oscillations of an air column are investigated experimentally in a closed, straight tube of uniform cross-section with a so-called stack installed and subjected to a temperature gradient axially. The stack consists of many through pores axially and it is sandwiched by hot and cold (kept at ambient temperature) heat exchangers so that a temperature gradient is imposed to yield axial heat flow.

The heat flow entering the stack from the hot heat exchanger flows down not only in the solid but also in the air toward the cold one and leaves there. The air in the stack is set in a thermally non-equilibrium state and the heat flow is always exposed to various disturbances so is fluctuating. As there exist eigenmodes of oscillations of the air column in the tube, it is possible that one of the modes may be excited to give rise to instability. However because dissipative effects by viscosity and thermal conductivity are present, they usually act to suppress the instability so that the quiescent state appears to be maintained.

As the temperature gradient becomes steeper and the magnitude of the heat flow becomes greater, the dissipative effects no longer suppress the instability but rather promote it by taking energy from the heat flow. Such instability may be understood on the analogy of instability of viscous flow. The heat flux through the wall can give rise to instability if its phasing with the pressure variations is favorable. This corresponds to Rayleigh's criterion of instability in the first category, though the heat release rate is now replaced by the heat flux. For this instability to occur, there is a threshold of a heat flow, i.e. of a temperature gradient. This condition is a marginal condition of instability, which depends on each eigenmode of oscillations.

[1] sugimoto@me.es.osaka-u.ac.jp

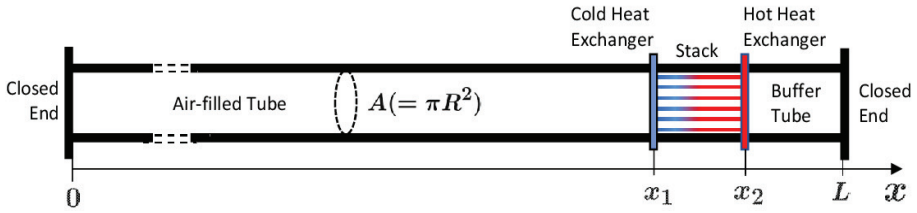

Figure 1 – Geometrical configuration of the tube.

When one of the eigenmodes becomes unstable, the amplitude grows exponentially. As it becomes larger, higher harmonics tend to be generated by nonlinearity and energy in the unstable mode is transferred to higher modes in a cascade manner. As a consequence, the amplitude of the unstable mode tends to be saturated and eventually self-excited, periodic oscillations emerge. The marginal conditions of instability are available based on Rott equation (see references in (2)). Optimization of the system for low onset temperature is studied in (3). When the oscillations enter a nonlinear regime, it is difficult to tackle them analytically.

In the following, the initial onset of instability to the emergence of the self-excited oscillations are demonstrated experimentally. The present experiments deal with the standing wave in the closed tube with ends, which is compared with the traveling wave in the looped tube without ends demonstrated previously in (4). So there are some overlaps in the experimental stet-ups and methods.

2. Experiments

Figure 1 illustrates schematically the geometrical configuration of the tube. The tube is of length L =3,630 mm and of diameter $2R = 80$ mm and is made of stainless steel. It is closed by flat plates on both ends and is filled with atmospheric air. A stack made of ceramics is installed in the tube and is sandwiched by hot and cold heat exchangers to impose a temperature gradient along the stack. The stack is of length 150 mm and of diameter 79 mm.

Taking the x axis along the tube from the left end, the cold and hot ends of the stack are located at x_1 =3,235 mm and x_2 =3,385 mm, respectively. The interval between x_2 and $x = L$ is called a thermal buffer tube over which the temperature decreases toward the right end. The two heat exchangers are almost the same as those used in the looped tube (4). Only difference is in structure of the hot heat exchanger. The slit plate with equally spaced 7 fins of thickness 2 mm and of axial depth 10 mm is replaced by a porous plate of axial depth 10 mm with regularly spaced pores of diameter 7.5 mm so that the porosity is 66%.

Four stacks are used and the geometry of the stacks is given in Tab. 1. Each stack has many through pores of square cross-section axially, which open regularly over the cross-section of the stack in the form of square cells. Each cell is of length $2H + 2W$ on a side and a square pore of length $2H$ on a side is located at the center of each cell. The porosity ϕ of the cell is given by $H^2/(H+W)^2$.

One end of the stack at $x = x_2$ is set in contact with the hot heat exchanger heated by a tubular heater wound around the outside of the heat exchanger. The stack is also heated from inside by a cartridge heater embedded along the centerline from the hot end. Both heaters are heated by following the protocol determined in advance to apply voltages (4). The other end of the stack is set in contact with the cold heat exchanger cooled by a tap water. Temperature of each heater is measured by a thermocouple embedded therein. The pressure is measured by pressure sensors flush mounted on the flat plate at both ends and at a location $x = x_3 = 1{,}800$ mm, which is close to the middle of the tube, i.e. the pressure node of linear oscillations in a uniform tube without a stack.

Table 1 – Geometry of the stacks

No. of cells [in^{-2}]	Pore width $2H$ [mm]	Wall thickness $2W$ [mm]	Porosity ϕ [%]	Remark [Materials]
50	3.0	0.80	62	Lithia
100	2.0	0.62	58	Lithia
200	1.5	0.30	69	Cordierite
300	1.2	0.27	67	Cordierite

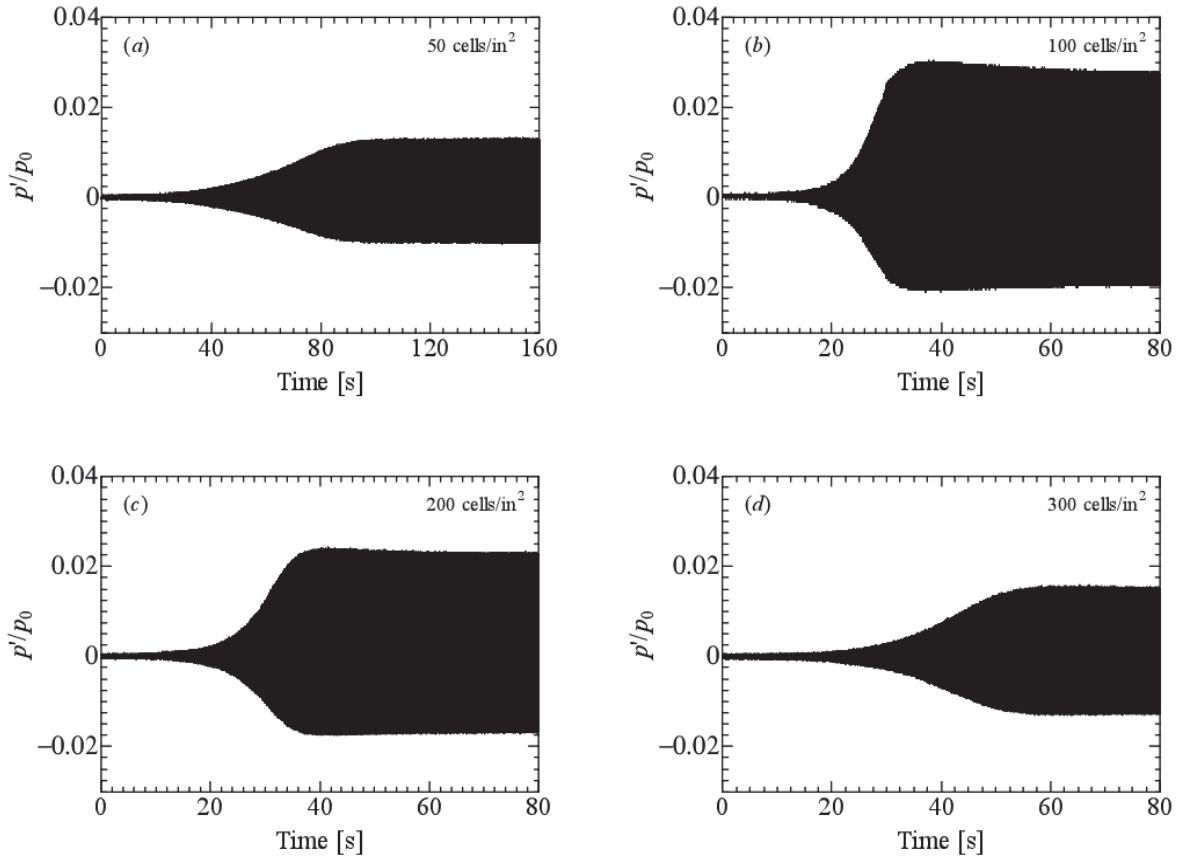

Figure 2 – Step-up behaviors of the excess pressure p' relative to the atmospheric one p_0 measured on the left end of the tube in the cases of the stacks 50, 100, 200 and 300 cells/in^2 in (*a*), (*b*), (*c*) and (*d*),

3. Results

After 2,600 to 2,900 s from the start of the experiment, the air column begins to oscillate spontaneously except for the case of 50 cells. Figure 2 shows the step-up behaviors of the excess pressure p' over the atmospheric one p_0 measured on the left end of the tube. The origin of the time in each figure is taken independently of the time set at the start of the experiment. Because of measurements over a long-time span 80 s or 160 s in (*a*), only envelopes of the amplitude of oscillations are visible.

The amplitude steps up the most rapidly in the case of 100cells and the most slowly in the case of 50 cells, where it takes 4,600 s for the step-up. It is noted that the temperature of either one (or both) of the heaters is observed to drop suddenly and sharply just before the beginning of the step-up observed. The same phenomena are also observed in the case of the looped tube (4).

In the course of time after the step-up, the amplitude increases gradually in response to the increase in the input powers to the heaters until 5,000 s. After this time, the temperatures of the heaters remain constant and the oscillations appear to reach a steady state by 7,200 s. Figure 3 displays the profiles of the excess pressure p' measured at 7,200 s on both ends and at $x = x_3$. The origin of the time is also arbitrarily taken. The blue and green curves represent the profiles measured at $x = 0$ and $x = L$, respectively. The red curve represents the one measured at $x = x_3$.

The profiles in blue and green exhibit typical characteristics of nonlinear oscillations. The crests are narrow and sharp, whereas the trough are flat and wide. Because the phase difference between the blue and green curves appears to be π, it is found that the oscillations occurs in the lowest 1/2-wave mode of oscillations where the tube length corresponds to the half wavelength. The mean pressure on both ends is found to be higher than p_0. The peak pressure on the right end in the buffer tube is seen to be slightly higher than that on the left end. The maximum in the peak-to-peak pressure is about 10% relative to p_0 on the right end. The maximum on the left end is slightly smaller than this value.

The period of oscillations can be read off from Fig.3 to be about 20 ms so that the frequency of oscillations is estimated to be about 50 Hz. Figure 4 shows the Fourier spectra of the profile measured on the left end in Fig. 3. It is found that the frequency of the first harmonics is 48.1 Hz and that many higher harmonics are visible up to the 20th one. Because the middle of the tube corresponds to the pressure node of linear

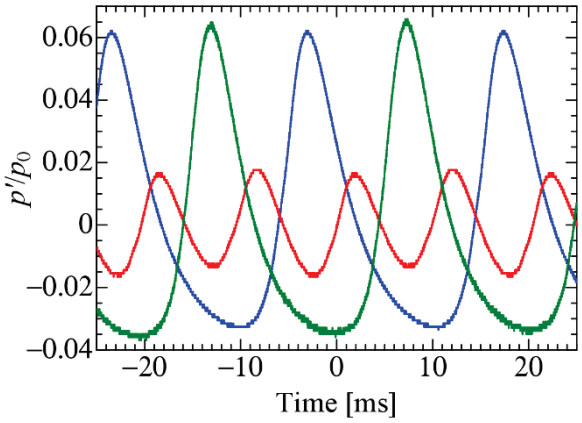

Figure 3 – Temporal profiles of p' relative to p_0 measured on the left end (blue) and the right end (green) at 7,200 s in the case of 100 cells where the profile in red represents the one at $x = x_3$ almost in the middle of the tube.

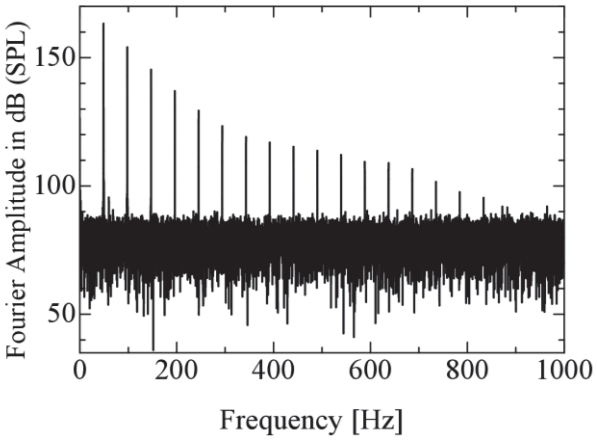

Figure 4 – Fourier spectra of the profile on the left end in Fig.3.

oscillations, the profile in red is due to the second-harmonic oscillations so that the amplitude is small.

4. Discussions

4.1 Marginal Conditions of Instability

It has been demonstrated that the instability of heat flow in the stack gives rise to self-excited oscillations of the air column in the closed tube. Marginal conditions of instability are available by using Rott equations. Assuming that the temperature in the stack increases exponentially from $x = x_1$ toward $x = x_2$ and then decreases in the buffer tube toward the closed end in the form of a quadratic function, the marginal conditions are calculated for the porosity ϕ of the stack from 0.5 to 0.9 by step 0.1 (2). Figure 5 shows the ratio of the highest temperature T_H at $x = x_2$ to the ambient temperature T_0 in $0 \le x \le x_1$ against the pore radius R_s of the stack. For the square pore, R_s is taken as a hydraulic radius defined by twice the area $4H^2$ divided by the wetted perimeter $8H$ so that $R_s = H$.

It is seen in Fig.5 that the porosity has little effects on the marginal conditions. This is different from the case of the looped tube (2). More importantly, the marginal condition suggests that there is a lower bound of the pore radius so that no instability occurs for the pore radius smaller than 0.4 mm. The solid circle, triangle, square and diamond represent, respectively, the temperature ratios T_H/T_0 measured at the onset of instability. Because the stack is heated by the two heaters, the mean temperature is used for T_H (4). For all stacks, the temperature ratios measured are higher than the ones predicted by the marginal conditions. However the tendency of the marginal curves is seen in the data plotted, namely, they appear to lie on a curve convex downward and the radius of the minimum temperature ratio appears to coincide. The ratios are comparable with those in the looped tube (4).

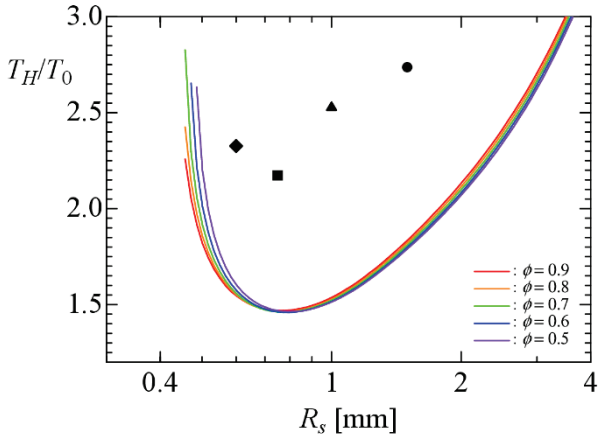

Figure 5 – Marginal conditions for the temperature ratio T_H/T_0 against the pore radius R_s for the porosity ϕ from 0.5 to 0.9 by step 0.1, where the solid circle, triangle, square and diamond represent the temperature ratios measured at the onset of instability in the cases of 50, 100, 200 and 300 cells shown in Fig.2, respectively.

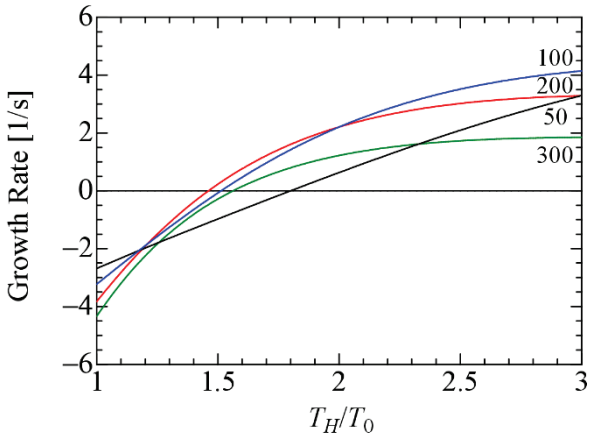

Figure 6 – Linear growth rate against the temperature ratio T_H/T_0 in the cases of 50, 100, 200 and 300 cells.

4.2 Linear Growth Rate

Next the linear growth rate is calculated when the temperature ratio exceeds the marginal one. Figure 6 shows the growth rate [s^{-1}] against T_H/T_0. Just on the marginal curves in Fig.5, the growth rate vanishes and becomes positive above them. It is found that the rate is greatest in the case of 200 cells for T_H/T_0 less than 2 and in the case of 100 cells above it. This is consistent with the rapid step-up behavior in these cases. In the cases of 50 and 300 cells, on the other hand, the step-up is slow. From Fig, 5, it is found that the minimum temperature ratio is about 1.45 at $R_s = 0.75$ mm, which is close to the case of the stack of 200 cells.

Yu and Jaworski (3) give the optimum conditions for the low onset temperature in the case of a very short stack by assuming helium. Denoting a wavelength by λ, the stack should be located at $x - L/2 \approx 5.5\lambda/32$ for a circular pore. When λ is taken to be $2L$, the optimum position of the stack is at $x \approx 0.84L$. If the position of the stack in our experiment is taken as the middle of the stack as $x = x_s = (x_1 + x_2)/2$, $x_s \approx 0.91L$, which is closer to the right end. On the other hand, the optimum ratio $r_h/\delta_k \approx 1.0$ where $r_h = R_s/2$ and δ_k is the thermal penetration depth. This depth is estimated to be 0.35 mm for air, and the optimal radius R_s is 0.72 mm. This value is close to the radius at the minimum temperature ratio in Fig.5 and is close to the case of the stack of 200 cells. This is also seen in Fig.6.

The growth rate calculated is greater than that measured from the step-up behavior in Fig.2. It is conjectured that the step-up in Fig.2 is not caused by the linear instability. Because the envelopes of the pressure profiles in Fig.2 are asymmetric in polarity, the oscillations are not in a linear regime of instability growing exponentially. Rather the linear growth might have already occurred before the step-up shown. If so, the pressure smaller than 10^{-3} in magnitude should be measured but it cannot be captured by the pressure sensors used. According to the results of CFD for the looped tube (5), perhaps, the step-up behavior in Fig.2 will belong to the second regime of hierarchial spectral broadening subsequent to the first regime of the modal growth by the linear theory.

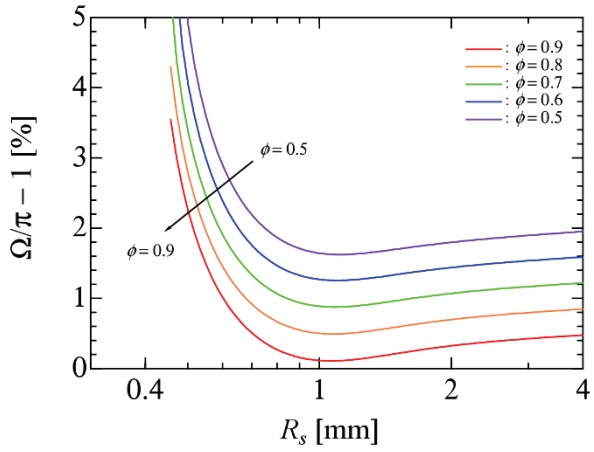

Figure 7 – Dimensionless angular frequency Ω relative to π of the marginal oscillations for the porosity from 0.5 to 0.9 by step 0.1.

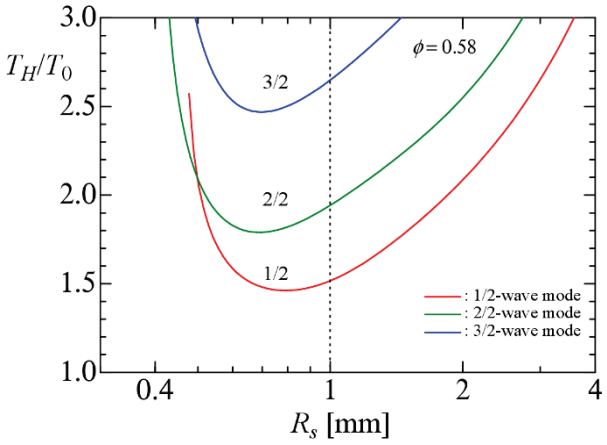

Figure 8 – Marginal conditions for the temperature ratio T_H/T_0 against the pore radius R_s for the 1/2-wave to the 3/2-wave modes for the porosity 0.58 where the dotted line designates the case of the stack of 100 cells.

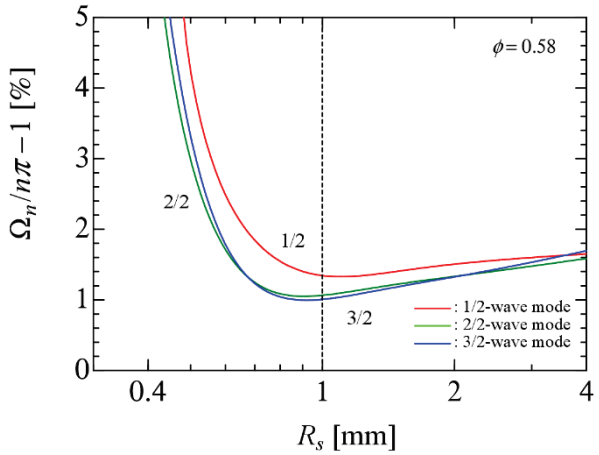

Figure 9 – Dimensionless angular frequency of the marginal oscillations $\Omega_n (= L\omega_n/a_0; n = 1,2,3)$ for the 1/2-wave to the 3/2-wave modes for the porosity 0.58 where the dotted line designates the case of the stack of 100 cells.

4.3 Angular Frequency of Marginal Oscillations

The angular frequency of the marginal oscillations is also available. The oscillations take place in the lowest 1/2-wave mode so the dimensionless angular frequency $\Omega\,(=L\omega/a_0)$ is nearly equal to π, ω and a_0 being, respectively, a dimensional angular frequency and sound speed. Figure 7 shows how far Ω deviates in percentage from π in the lossless case without a stack. It is found that as the porosity increases, Ω approaches π, while as the pore radius becomes smaller so that the dissipative effects are enhanced, it tends to deviate significantly from it.

4.4 Marginal Conditions of Higher Modes and Degree of Dissonance

As the self-excited oscillations take place at the temperature ratio higher than the one given by the marginal condition, higher modes are also excited. Figure 8 shows the marginal conditions of the 1/2-wave to the 3/2-wave modes against the pore radius with the porosity fixed at 0.58 where the dotted line designates the case of 100 cells. If the temperature ratio exceeds 2.5, the 1/2-wave to the 3/2-modes are unstable.

The angular frequencies in the higher modes are also available. Denoting the dimensionless angular frequency of the n/2-wave mode by $\Omega_n\ (=L\omega_n/a_0, n=1,2,3)$, ω_n being the dimensional angular frequency in the n/2-wave mode, Ω_n are close to $n\pi$. In the lossless case without a stack, Ω_n are n-multiples of π. Then the tube is consonant. Figure 9 shows how far Ω_n deviate from $n\pi$. In other words, it shows the degree of dissonance.

As the amplitude of oscillations becomes large in the consonant tube, frequencies of all higher harmonics coincide with those of higher modes so that the higher modes are easily excited. Then the energy in the unstable modes is transferred to higher modes and eventually a shock wave appears. In the present experiments, however, no shock wave appears. This is compared with the case of the looped tube where the shock wave appears (4). Checking the degree of dissonance in both cases, this is larger in the present case. Thus this subtle difference is thought to determine whether or not the shock wave emerges.

4.5 Mode of Oscillations

Finally the axial variations of the excess pressure and the axial mass flux density due to the marginal oscillations in the 1/2-wave mode are displayed for the porosity 0.58 and $R_s = 1.0\,\mathrm{mm}$ in the case of 100 cells. The pressure is assumed to be uniform over the cross-section, while the mass flux density $\rho_e u'$ is non-uniform and averaged over it, where ρ_e and u' denote, respectively, the density in the quiescent state and the axial velocity. Letting the excess pressure and the mean axial mass flux density to be in the form of $\mathrm{Re}\{P(x)\exp(\mathrm{i}\omega t)\}$ and $\mathrm{Re}\{F(x)\exp(\mathrm{i}\omega t)\}$, Fig.10 shows the absolute values of the complex amplitudes P and F. In addition, the distribution of the mean axial energy flux density (intensity) $I\ (=\mathrm{Re}\{PF^*\}/2\rho_e)$ averaged over the period of oscillations is also drawn, the asterisk designating the complex conjugate.

The amplitude profiles of $|P|$ and $|F|$ appear to be almost the same as those in the 1/2-wave mode of lossless oscillations in a uniform tube without a stack. Here P is normalized by $P(0)$. It is seen that $P(L)$ is slightly greater than $P(0)$. Although $|F|$ and I are discontinuous at both ends of the stack, they are continuous on multiplying the porosity. While I vanishes everywhere in the lossless standing wave, it decreases from zero on the left end toward the cold end of the stack due to the dissipative effects. However $I\phi$ increases across the stack up to the hot end of the stack and then decreases to vanish on the right end. It is seen that the energy flux is produced in the stack and flows out axially in the positive and negative senses.

In Fig.10, no information on phases is available. Figure 11 shows the real and imaginary parts of P and F in the solid and broken curves, respectively. The real parts correspond to the profiles at $\omega t = m\pi\ (m=1,2,3,...)$, while the imaginary parts to those at $\omega t = (m+1/2)\pi\ (m=1,2,3,...)$. It is found that the behaviors in the vicinity of the stack are different from those in the lossless case.

The profiles in Figs.10 and 11 are only in the case of the 1/2-wave mode. The self-excited oscillations observed include some unstable (active) modes of oscillations, while the remaining modes are passive. Thus the oscillations may be represented by the sum of the active and passive modes. When nonlinear interactions between them are taken into account, it is expected that the self-excited oscillations will be described analytically.

5 CONCLUSIONS

Thermoacoustic instability and ensuing self-excited oscillations have been demonstrated experimentally in the air-filled, closed tube with the stack subjected to the temperature gradient. It is remarked that there exists the lower bound of the pore radius for the instability to occur. Also remarked are no influences of the porosity on the marginal conditions. These are different from the case of the looped tube. The frequency in the present case is just twice as high compared with the one in the looped tube so that the thickness of diffusion layers is relatively thin. Nevertheless the pore radius for the instability is larger.

The degree of dissonance in the closed tube is larger and therefore no shock wave appears unlike in the

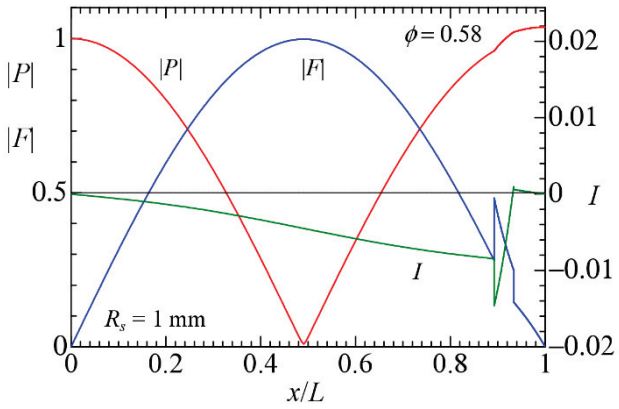

Figure 10 – Axial variations of the amplitudes of the excess pressure $|P|$ and of the axial mass flux density $|F|$ together with the variation of the mean axial energy flux density (intensity) I over the period in the 1/2-wave mode for the porosity 0.58 and $R_s = 1.0$ mm in the case of 100 cells.

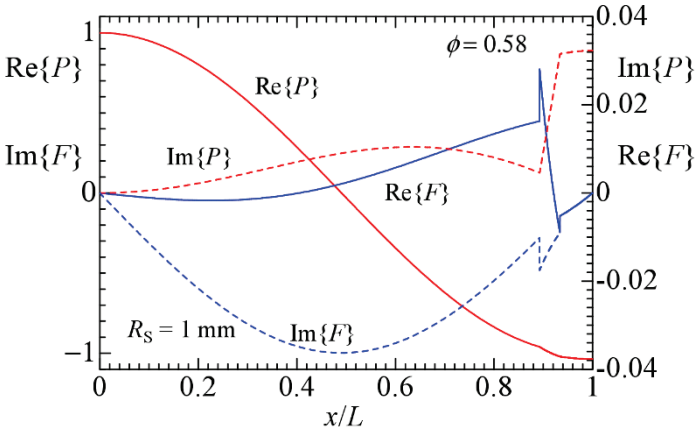

Figure 11 – Axial variations of the real and imaginary parts of the complex amplitudes P and F in the 1/2-wave mode for the porosity 0.58 and $R_s = 1.0$ mm in the case of 100 cells.

case of the looped tube. In spite of the oscillations free from the shock, however, the maximum peak-to-peak pressure of 10% is smaller than 15% in the looped tube. The low temperature ratio for the onset of instability is important from a viewpoint of application, while larger amplitude of emergent self-exited oscillations is also desired. It is remarked that the pore radius for the minimum temperature ratio does not coincide with that of the maximum growth rate and the large amplitude of emergent oscillations.

ACKNOWLEDGEMENTS

The authors acknowledge the financial supports of Grant-in-Aide for Scientific Research (KAKENHI No. 26289036 and No. 18H01375) by the Japan Society for the Promotion of Science.

REFERENCES

1. Lawn, CJ, Penelet, G. Common features in the thermoacoustics of flames and engines. Int. J. Spray and Combust. 2018;10(1):3-37.
2. Sugimoto, N. Marginal conditions for the onset of thermoacoustic oscillations due to instability of heat flow. IMA J. Appl. Math. 2019;84:118-144.
3. Yu, Z, Jaworski, AJ. Optimization of thermoacoustic stacks for low onset temperature engines. Proc. IMechE Part A: J. Power Energy. 2010;224(3):329-337.
4. Sugimoto, N., Minamigawa, K. Experiments on self-excited thermoacoustic oscillations in an air-filled looped tube with a pair of stacks. J. Phys. Soc. Jpn. 2018;87:104401 1-12.
5. Gupta, P., Lodato, G., Scalo, C. Spectral energy cascade in thermoacoustic shock waves. J. Fluid Mech. 2017;831:358-393.